CARBON 87 (2015) 358–364

Available at www.sciencedirect.com

ScienceDirect

journal homepage: www.elsevier.com/locate/carbon

Graphite melting: Atomistic kinetics bridges theory and experiment

N.D. Orekhov [a,b], V.V. Stegailov [a,b,c,*]

[a] Joint Institute for High Temperatures of RAS, Izhorskaya st. 13 bldg. 2, 125412 Moscow, Russia
[b] Moscow Institute of Physics and Technology, Institutskiy per. 9, 141700 Dolgoprudny, Russia
[c] National Research University Higher School of Economics, Myasnizkaya st. 20, 101000 Moscow, Russia

ARTICLE INFO

Article history:
Received 27 August 2014
Accepted 13 February 2015
Available online 21 February 2015

ABSTRACT

The graphite melting temperature remains poorly determined despite the considerable effort accomplished since the work of Bundy (1963) [1]. The absence of a consensus on its melting temperature at normal conditions has been considered as a technical problem that motivated more and more sophisticated experiments. The experimental evidences of the maximum on the graphite melting curve resulted in the liquid–liquid phase transition hypothesis for liquid carbon. However this hypothesis still requires a sound evidence. In this work using atomistic methods we focus on the kinetics of graphite melting and show that the experimental puzzles can be resolved by considering the graphite melting as a process in the non-equilibrium superheated solid. The unusually slow melting kinetics results in the existence of the superheated graphite at the microsecond timescale and thus biases the measurements of its equilibrium melting temperature.

1. Introduction

Graphite is the most refractory single element solid. Despite its abundance and importance the graphite melting temperature T_m remains a subject of controversy. The variation of the experimentally measured T_m values is more than 1000 K [1–14] (Fig. 1). In the context of the carbon phase diagram description the graphite melting temperature was once taken either as 3800 K [15], or as 5000 K [16]. The reviews of A.I. Savvatimskiy published in 2003 and 2005 [13,17] critically summarize the results of the three decades of experimental studies marked by outstanding achievements. The main polemical discourse of these reviews is connected with resolving the long-standing discrepancy in the experimentally measured values for the melting temperature of graphite. The T_m values tend to group in the low temperature and high temperature sets. The experiments based on pulse electrical discharge or fast laser heating [5,6,8,12–14] provide the group of the higher values about 4800 K. The group of lower values of T_m near 4000 K corresponds to moderate heating rates and is represented by the following works [1–4,9,11]. Some works [7,10] give the T_m values in between. The lower values of the graphite melting temperature have two interpretations: they are either connected with slow experimental heating rates and assumed to be more accurate as advocated by [18,19] or explained by the deficiencies of the measurement procedures and therefore considered as less accurate [13,17]. A possible existence of the dependency between the heating rate and the measured melting temperatures has been briefly discussed before, e.g.

---

* *Corresponding author at:* Joint Institute for High Temperatures of RAS, Izhorskaya st. 13 bldg. 2, 125412 Moscow, Russia.
E-mail addresses: nikita.orekhov@gmail.com (N.D. Orekhov), stegailov@gmail.com, vstegailov@hse.ru (V.V. Stegailov).
http://dx.doi.org/10.1016/j.carbon.2015.02.049
0008-6223/© 2015 Elsevier Ltd. All rights reserved.

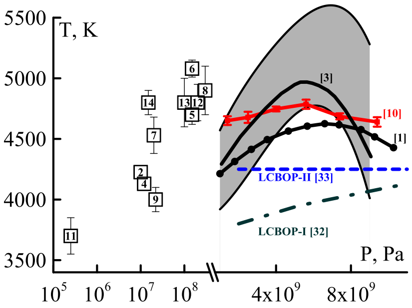

Fig. 1 – The experimental results on the graphite melting temperature in two pressure ranges from different experiments [1–14] (the numbers match the corresponding citations in the reference list). The data from [3] are shown as the average line as well as the upper and lower envelope curves that show the scatter of the individual measurement results. The results of atomistic calculations for LCBOP-I [36] and LCBOP-II models [37] are shown as well. (A colour version of this figure can be viewed online.)

in [18,14,20], but has not obtained much support among the scientific community.

The pressure dependence of the graphite melting curve provided an additional puzzle. All of the existing experiments [1,3,10] indicated that the graphite melting curve had a maximum around 5–6 GPa. The interpretation of the maximum is connected with the possible liquid–liquid phase transition (LLPT) in liquid carbon similarly to other substances [21,22].

Liquid carbon was studied in the pioneering works at the dawn of the *ab initio* molecular dynamics (MD) [23,24] that provided a certain evidence of the coordination changes in liquid carbon at 100 GPa and hence supported the LLPT hypothesis. The equations of state for carbon that reproduced the LLPT in the graphite melting pressure range were developed [25,26]. The subsequent *ab initio* studies of the carbon phase diagram showed a maximum at the diamond melting curve but did not confirm the LLPT hypothesis for the corresponding ultrahigh pressures [27,28]. The next equation of state models for carbon were focused at extreme conditions [29,30]. Atomistic simulation methods became mature enough to handle the graphite melting problem as soon as the sophisticated interatomic potentials for carbon had been created (AIREBO [31] and LCBOP [32]). However despite considerable effort no confirmation of the LLPT in liquid carbon was found [33–35]. The pressure dependencies of the graphite melting temperature calculated for the LCBOP type models using thermodynamic integration [36,37] are located in the region 3800–4250 K and display no evidence of the maximum (see Fig. 1). Therefore the nature of the observed maximum of the melting curve remains unexplained.

It is well known that solids can not be essentially superheated in experiments due to rapid heterogeneous melting on defects of crystal structure (e.g. [38,39]). Superheating can be barely detectable in ultrafast experiments [40,41] when homogeneous nucleation becomes the limiting factor. Despite this consensus the problems with the graphite melting temperature determination have motivated us for the careful study of its melting kinetics in the superheated solid state that is reported in this work.

2. Melting front propagation (heterogeneous nucleation)

In our calculations we use the reactive empirical bond-order potential AIREBO [31]. This model describes both the strong short-range interatomic interactions within basal ("graphene") layers and the weak long-range interaction between them. We consider the heterogeneous melting at the solid–liquid phase boundary and the homogeneous nucleation of melt in bulk graphite at high degrees of superheating.

To study the kinetics of heterogeneous process melting front velocity calculations are carried out using the two-phase simulation method (e.g. [42–44]). The simulation box is approximately 20 Åin *x* and *y* directions and 120 Åin the z direction (about 7000 atoms). The 3D periodic boundary conditions (PBC) are applied. LAMMPS is used for MD simulations [45,46]. Initially atoms of the crystal phase in a part of the simulation box are kept frozen, while the rest of the system is heated up to its complete melting. The simulation box is then equilibrated towards the target temperature and pressure for 0.5 ns. The MD time step is 0.1 fs. After equilibration, modeling of the melting front propagation is performed in the *NPT* ensemble [47]. We consider two variants of the crystal orientation: the melting front normal to the basal graphite plane (Fig. 2(⊥)) and the melting front parallel to the basal plane (Fig. 2(||)).

In the considered range of temperatures (4100–4700 K) we observe a steady motion of the phase boundary (Fig. 2). In all cases the melting front maintains its flat structure. Front velocities are calculated by linear interpolation. An average

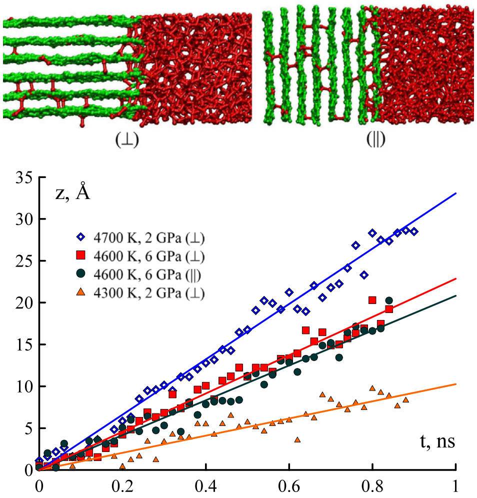

Fig. 2 – The ball-stick models represent two solid–liquid interface orientations considered in this work. Atoms of graphene layers are green, liquid-like atoms and *sp*^{3}–*sp*^{3} cross-link defects are shown in red. The melting front motion with time is illustrated on the plot for different temperatures. For *T* = 4600 K the data for two surface orientations are compared. (A colour version of this figure can be viewed online.)

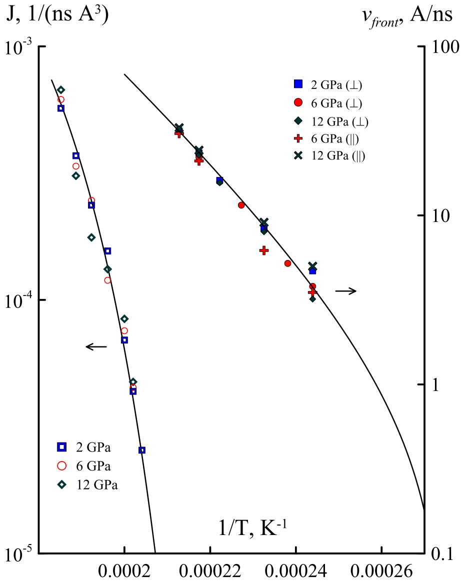

Fig. 3 – The dependence of the melting front velocity v_{front} (at different front orientations) and the homogeneous nucleation rate *J* on the inverse temperature for different pressures. The solid lines represent fitting by Eqs. (1) and (2) (see text). (A colour version of this figure can be viewed online.)

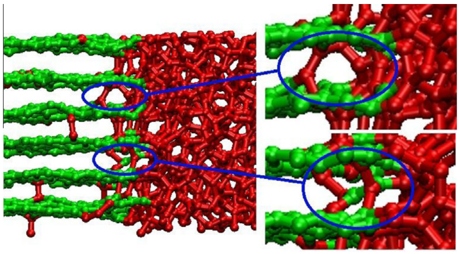

Fig. 4 – A part of the simulation box with the phase boundary. Atoms of graphite layers are shown in green, atoms with other coordinations (disordered structure, interstitials) are shown in red. (A colour version of this figure can be viewed online.)

duration of MD trajectories is about 1 ns depending on temperature.

The results of the melting front velocity calculations for various pressures, temperatures and front orientations are summarized on Fig. 3. At $T = 3700$–3750 K we do not observe any unidirectional motion of the phase boundary on the timescale up to 5 ns. It is possible to observe the front propagation for $T < 4000$ K, however after the careful examination we have found out that the ambiguity of v_{front} values at these T is larger than we estimated preliminary [48]. With the better statistics than presented in [48] now we cannot resolve any dependence of the melting front velocity on pressure.

Due to the exponential decrease of v_{front} with temperature the computational constraints do not allow us to determine the equilibrium melting point from the condition $v_{front} = 0$. For this purpose we have conducted thermodynamic integration calculations using the technique proposed in [49], and for $P = 6$ GPa obtained $T_m = 3640 \pm 150$ K . The precision of this estimate of the equilibrium melting temperature is limited by the significant basal planes waving with respect to the immobile reference "Einstein crystal" lattice. This effect differs from the layer sliding discussed in [37] that we have similarly overcome by fixing each layer's center of mass. The difference between our value of T_m for the AIREBO model and the result for the LCBOP-II model [37] is about 500 K and most probably stems from the difference of the potentials.

The kinetics of melting of simple solids is known to be similar to the crystallization kinetics and is governed by the average thermal velocity of atoms $v_{th} = (3k_BT/m)^{1/2}$ [50–52,42], i.e. $v_{front}/v_{th} \simeq \Delta T/T$, where $\Delta T = T - T_m$. However we see that the melting front propagation in graphite is very slow ($v_{front}/v_{th} \sim 10^{-4}$ at $\Delta T/T \sim 0.1$) and has a distinct exponential dependence on temperature (Fig. 3). Therefore in this case we apply the quasi-equilibrium model for the rate of a first-order phase change [53]:

$$v_{front}(T) = \frac{ak_BT_D}{h}\left[\exp\left(\frac{\Delta G_m}{k_BT}\right) - 1\right]\exp\left(-\frac{W_f}{k_BT}\right), \tag{1}$$

where k_B is the Boltzmann constant, h is the Planck constant. For the estimate of ak_BT_D/h we take the corresponding Debye temperatures [54] and lattice distances: $T_D = 2500$ K and $a = 1.23$ Å for the (⊥) orientation and 950 K and 3.35 Å for the (||) orientation that give the values of $(6.4$–$6.6)10^4$ Å/ns. $\Delta G_m = L\Delta T/T_m$ is the free energy difference between solid and liquid phases ($L = 120$ kJ/mol is the heat of fusion). The only remaining unknown constant W_f is the energy barrier for the atom "detachment" from solid into liquid. The MD results fitting with Eq. (1) gives $W_f \simeq 3.25$ eV. A visual inspection of the "detachment" events reveals their connection with the formation of the interplanar interstitial-like defects at the solid side of the melting front (see Fig. 4). The formation energies from 5.5 to 8.0 eV were obtained in the static *ab initio* calculations of different interstitial defects in graphite [55]. The value of W_f is therefore quite reasonable, taking into account that it corresponds to the high temperature system with strong thermal fluctuations, basal planes oscillations and presence of the disordered phase.

The crystallization process is apparently even more sluggish than melting. At the MD timescale considered we observe no crystallization at $T < 3700$ K .

3. Homogeneous nucleation

The homogeneous nucleation rate in highly metastable states can be directly calculated via MD method using ensemble averaging (e.g. [56–58]). We consider a graphite crystal lattice of 3360 atoms in the cubic MD simulation box ($V \simeq 30^3$ Å^3) in the 3D PBC. Starting with the perfect crystal we follow atom dynamics in the *NPT* ensemble [47] for the selected $T \geqslant 4900$ K temperatures. For each temperature the time t_{nucl} before the first critical nucleus appears in the simulation box is calculated as an average over 5–7 trajectories. The corresponding homogeneous nucleation rate is $J = 1/(t_{nucl}V)$ (Fig. 3). According to the classical nucleation theory (CNT):

$$J(T) = J_0 \exp\left(-\frac{W_n}{k_B T}\right), W_n = \frac{16\pi\sigma^3}{3(\Delta G_m)^2}, \quad (2)$$

where W_n is the free energy of the critical nucleus formation. In the CNT σ stands for the solid–liquid interface energy. Here we consider σ and J_0 as unknown parameters and find them by fitting the MD data (Fig. 3). Our MD calculations show no evident dependence of J on pressure for 2–12 GPa (as well as for $\upsilon_{front}(T)$).

4. Mesoscopic model of graphite melting

Now having the information on the kinetics of two basic mechanisms of graphite melting we are able to describe how melting proceeds in macroscopic samples heated at different heating rates. Experimentally studied graphite specimens are polycrystallites of different grades. The average crystallite size essentially varies depending on the manufacturing procedure (e.g., according to [17] a typical crystallite size λ in well-prepared HOPG is about 2 μm, in [14] the crystallite size was 10–20 μm).

As the heating of the sample proceeds liquid phase begins to form at $T > T_m$ via the melting front propagation from grain boundaries and other types of defects (heterogeneous nucleation). Homogeneous nucleation becomes important in the course of the specimen heating if an essential part of the specimen still remains solid at a sufficient superheating degree $\Delta T/T_m \sim 0.2$. Below we propose a model how the volume of the liquid phase grows in time via both mechanisms depending on the rate of the specimen heating.

The growth of liquid phase due to melting front propagation from grain boundaries can be described as

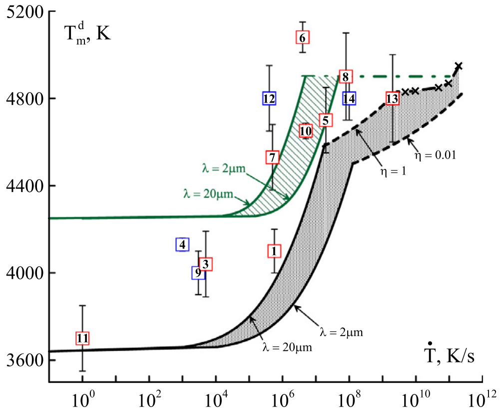

Fig. 5 – The dependence of the graphite melting temperature *detected in experiment* on the heating rate. The symbols meaning is as on Fig. 1 (here red shows electrical and blue shows laser heating experiments). The solid lines show the region of $T_m^d(\dot{T})$ determined by Eq. (5) for the average grain size $\lambda = 2$–20 μm. The dashed lines show the region determined by Eq. (6) for the critical liquid phase fraction $\eta = 0.01$–1. The black curves are our results for AIREBO and the green curves are our estimates for LCBOP-II (without data for homogeneous nucleation). The dash-dotted lines show the graphene melting determined in this work (the crosses) and in [59]. (A colour version of this figure can be viewed online.)

$$\frac{dV_{liq}}{dt} = S(t)\upsilon(T(t)) \propto (V_0 - V_{liq})^{2/3}\upsilon_{front}(T(t)), \quad (3)$$

where $V_0 \propto \lambda^3$ is the initial crystallite volume, $S(t) \propto \lambda^2$ is the area of the crystallite surface, t is the time from the moment temperature T_m has been reached ($T = T_m + \dot{T}t$, where $\dot{T}$ is the heating rate). In pulse-heating experiments the beginning of specimen melting is usually detected by the macroscopic parameters measurements: e.g. in the electrical heating experiments the resistance and inserted energy dependencies on time are recorded, in the laser heating experiments the time dependence of temperature in the heating zone is obtained. Noticeable features on such dependencies are interpreted as the results of the formation of the significant amount of liquid as T_m is reached. Considering the possibility of superheating in this work we distinguish the thermodynamic melting temperature T_m and the melting temperature *detected in experiments* $T_m^d = T_m + \dot{T}t_m$, where t_m is a moment when a detectable amount of liquid phase appears. After the integration of Eq. (3) from $t = 0$ to $t = t_m$ we get

$$\int_0^{V_0} \frac{dV_{liq}}{(V_0 - V_{liq})^{2/3}} = \int_{T_m}^{T_m^d} \upsilon_{front}(T(t))dt, \quad (4)$$

and obtain the dependence $T_m^d(\dot{T})$ in the implicit form

$$\dot{T} = \frac{1}{3\lambda}\int_{T_m}^{T_m^d} \upsilon_{front}(T)dT. \quad (5)$$

The role of the homogeneous nucleation in the growth of liquid phase becomes comparable to the effects of the heterogeneous mechanism at $T > 4300$–4400 K. Here we take into account only homogeneous nucleation events and do not consider the growth of nuclei. This assumption is justified by the small υ_{front} values and by the fast exponential growth of $J(T)$ with temperature. Integrating Eq. (2) from T_m up to the moment when the critical fraction of liquid phase η is reached, we get

$$\dot{T} = \frac{V_{nucl}}{\eta}\int_{T_m}^{T_m^d} J(T)dT, \quad (6)$$

where V_{nucl} is the critical nucleus volume (that can be estimated as 1 nm^3 according to the MD results). To compensate the neglection of nuclei growth we consider the wide range of $\eta = 0.01$–1.

The numerical solutions of Eqs. (5) and (6) are shown on Fig. 5 with the parameters $T_m = 3640$ K for AIREBO and $T_m = 4250$ K for LCBOP-II [37]. One can see that there are two ranges of heating rates. At $\dot{T} \lesssim 10^6$ K/s melting is determined by the melting front propagation and temperatures close to the equilibrium melting temperature T_m are expected to be detected in experiments. At $\dot{T} \gtrsim 10^8$ K/s melting is determined by homogeneous nucleation and the melting temperature *detected in experiments* becomes close to the limit of the single graphene layer stability. Our calculations of the decay (or melting) temperature for a 4000-atom graphene layer (the black crosses on Fig. 5) match both the $T_m(\dot{T})$ zone of bulk graphite homogeneous melting and the results from [59].

Fig. 5 shows that the model estimates are in a good agreement with the experimental data from the laser and electrical current heating experiments [1–14].

5. Discussion

At this moment we cannot establish a “true” equilibrium graphite melting temperature using the classical MD models only: the difference between the AIREBO and LCBOP-II T_m values shows the magnitude of the uncertainty due to the empirical nature of these interatomic potential models. Nevertheless both models show significant variation of T_m^d with $\dot{T}$, comparable to the experimental variation $T_m = 3700$–$5000\,\mathrm{K}$. The melting temperatures obtained by thermodynamic integration in the infinite-time approximation are 3640 K for AIREBO, 3800–4100 K for LCBOP-I [36] and 4250 K for LCBOP-II [37]). The results of the graphene layer melting temperature calculations at a constant heating rate are 4900–4950 K for LCBOP-II [59] and 4800–4900 K for AIREBO (this work). Therefore the scatter of the measured T_m values can be explained by the ease of graphite superheating due to its unusually slow melting kinetics.

The revealed graphite melting kinetics can shed light on the nature of the maximum of its melting curve (Fig. 1). It is known that at least in two [1,10] of the three corresponding experimental studies [1,3,10] the authors used low density graphite samples (1.6 g/cc). At the length scale of individual grains the microscopic porosity of the specimen looks like a microstructure with some empty space between grains. Thus the initial energy deposition that increases T and P should simultaneously decrease this empty volume by expanding the grains. This expansion results in the increase of the interlayer spacings between graphite sheets that increases W_f and slows down melting kinetics. The decrease of microscopic porosity can explain the rise of the melting temperature T_m^d *detected in experiments* up to a certain pressure (e.g. 5–6 GPa). The further increase in pressure results in the increase of density at the individual grains level that primarily decreases the interplanar distance in graphite, lowers W_f and hence lowers T_m^d. This explanation does not require an assumption about a LLPT in liquid carbon and implies that the melting curve maximum is a kinetic effect that depends on the specimen microstructure.

6. Conclusions

Using the molecular-dynamics method we have shown that melting in graphite proceeds much slower than in other solids. We have calculated the rates of heterogeneous and homogeneous melting mechanisms as well as the thermodynamic melting temperature of graphite and the single graphene layer decay temperature for the AIREBO interatomic potential. These results combined in a simple mesoscopic model that takes into account a typical microstructure of graphite specimens, have allowed us to describe a large set of experimental results on the detected graphite melting temperatures at different heating rates. These results suggest that at the heating rates higher that $\sim 10^6$ K/s graphite specimens in most cases become superheated, the solid–liquid transition temperature becomes higher than the equilibrium melting temperature and is influenced mainly by the specimen microstructure and the energy deposition process. The slow melting kinetics of graphite together with the pressure and temperature effects on porosity of commonly used graphite specimens can explain the observed maximum on the experimentally detected melting temperature dependence on pressure as a kinetic effect without the hypothesis about a liquid–liquid phase transition in liquid carbon.

Acknowledgments

The work was financially supported by the Russian Science Foundation (Grant No. 14-19-01487). The authors are grateful to A.I. Savvatimskiy and A.Yu. Basharin for their interest in this study.

Appendix A. Supplementary data

Supplementary data associated with this article can be found, in the online version, at http://dx.doi.org/10.1016/j.carbon.2015.02.049.

REFERENCES

[1] Bundy FP. Melting of graphite at very high pressure. J Chem Phys 1963;38(3):618–30. http://dx.doi.org/10.1063/1.1733715.

[2] Schoessow GJ. Graphite triple point and solidus–liquidus interface experimentally determined up to 1000 atm. Phys Rev Lett 1968;21(11):738.

[3] Fateeva NS, Vereshchagin LF. Concerning the melting point of graphite up to 90 kbar. JETP Lett 1971;13:110.

[4] Gokcen NA, Chang ET, Poston TM, Spencer DJ. Determination of graphite–liquid–vapor triple point by laser heating. High Temp Sci 1976;8:81.

[5] Sheindlin MA, Senchenko VN. Experimental investigation of graphite thermodynamic properties in the vicinity of melting point. Sov Phys Dokl 1988;298(6):1383–6.

[6] Baitin AV, Lebedev AA, Romanenko SV, Senchenko VN, Sheindlin MA. The melting point and optical properties of solid and liquid carbon at pressures of up to 2 kbar. High Temp High Press 1990;22(2):157–70.

[7] Cezairliyan A, Miiller AP. Measurement of the radiance temperature (at 655 nm) of melting graphite near its triple point by a pulse-heating technique. Int J Thermophys 1990;11(4):643–51. http://dx.doi.org/10.1007/BF01184334.

[8] Pottlacher G, Hixson RS, Melnitzky S, Kaschnitz E, Winkler MA, Jäger H. Thermophysical properties of POCO AXF-5Q graphite up to melting. Thermochim Acta 1993;218:183–93. http://dx.doi.org/10.1016/0040-6031(93)80421-6.

[9] Asinovskij EI, Kirillin AV, Kostanovskij AV. Phase diagram of carbon in the vicinity of the solid–liquid–vapor triple point. High Temp 1997;35(5):716–21.

[10] Togaya M. Pressure dependences of the melting temperature of graphite and the electrical resistivity of liquid carbon. Phys Rev Lett 1997;79(13):2474–7. http://dx.doi.org/10.1103/PhysRevLett.79.2474.

[11] Asinovskii EI, Kirillin AV, Kostanovskii AV, Fortov VE. Melting parameters of carbon. High Temp 1998;36(5):716–21.

[12] Musella M, Ronchi C, Brykin MV, Sheindlin MA. The molten state of graphite: an experimental study. J Appl Phys 1998;84(5):2530. http://dx.doi.org/10.1063/1.368414.

[13] Savvatimskii AI. Melting point of graphite and liquid carbon (concerning the paper ’experimental investigation of the thermal properties of carbon at high

temperatures and moderate pressures' by E.I. Asinovskii, A.V. Kirillin, and A.V. Kostanovskii). Phys Usp 2003;46(12):1295–303. http://dx.doi.org/10.1070/PU2003v046n12ABEH001699.

[14] Basharin AY, Brykin MV, Marin MY, Pakhomov IS, Sitnikov SF. Methods of increasing the measurement accuracy during the experimental determination of the melting point of graphite. High Temp 2004;42(1):60–7. http://dx.doi.org/10.1023/B:HITE.0000020092.25360.33.

[15] Whittaker AG. The controversial carbon solid–liquid–vapour triple point. Nature 1978;276(5689):695–6. http://dx.doi.org/10.1038/276695a0.

[16] Bundy FP, Bassett WA, Weathers MS, Hemley RJ, Mao HU, Goncharov AF. The pressure–temperature phase and transformation diagram for carbon; updated through 1994. Carbon 1996;34(2):141–53. http://dx.doi.org/10.1016/0008-6223(96)00170-4.

[17] Savvatimskiy AI. Measurements of the melting point of graphite and the properties of liquid carbon (a review for 1963–2003). Carbon 2005;43(6):1115–42. http://dx.doi.org/10.1016/j.carbon.2004.12.027.

[18] Asinovskii EI, Kirillin AV, Kostanovskii AV. Experimental investigation of the thermal properties of carbon at high temperatures and moderate pressures. Phys Usp 2002;45(8):869–82. http://dx.doi.org/10.1070/PU2002v045n08ABEH001110.

[19] Asinovskii EI, Kirillin AV, Kostanovskii AV. Once more about the experimental investigation of the thermal properties of carbon. Phys Usp 2003;46(12):1305–6. http://dx.doi.org/10.1070/PU2003v046n12ABEH001732.

[20] Klimovskii II, Markovets VV. The carbon phase diagram near the solid-liquid-vapor triple point. Int Sci J Altern Energy Ecol ISJAEE 2007;5(49):13–5. URL: http://isjaee.hydrogen.ru/pdf/AEE0507/ISJAEE05-07_Klimovskii.pdf.

[21] Rapoport E. Model for melting-curve maxima at high pressure. J Chem Phys 1967;46(8):2891–5. http://dx.doi.org/10.1063/1.1841150.

[22] Brazhkin VV, Popova SV, Voloshin RN. High-pressure transformations in simple melts. High Pressure Res 1997;15(5):267–305. http://dx.doi.org/10.1080/08957959708240477.

[23] Galli G, Martin RM, Car R, Parrinello M. Carbon: the nature of the liquid state. Phys Rev Lett 1989;63:988–91. http://dx.doi.org/10.1103/PhysRevLett.63.988.

[24] Galli G, Martin RM, Car R, Parrinello M. Melting of diamond at high pressure. Science 1990;250(4987):1547–9. http://dx.doi.org/10.1126/science.250.4987.1547.

[25] van Thiel M, Ree FH. High-pressure liquid–liquid phase change in carbon. Phys Rev B 1993;48:3591–9. http://dx.doi.org/10.1103/PhysRevB.48.3591.

[26] Fried L, Howard W. Explicit Gibbs free energy equation of state applied to the carbon phase diagram. Phys Rev B 2000;61(13):8734–43. http://dx.doi.org/10.1103/PhysRevB.61.8734.

[27] Wang X, Scandolo S, Car R. Carbon phase diagram from *ab initio* molecular dynamics. Phys Rev Lett 2005;95:185701. http://dx.doi.org/10.1103/PhysRevLett.95.185701.

[28] Correa AA, Bonev SA, Galli G. Carbon under extreme conditions: phase boundaries and electronic properties from first-principles theory. Proc Natl Acad Sci U S A 2006;103(5):1204–8. http://dx.doi.org/10.1073/pnas.0510489103. arXiv:http://www.pnas.org/content/103/5/1204.full.pdf+html, URL http://www.pnas.org/content/103/5/1204.abstract.

[29] Khishchenko K, Fortov V, Lomonosov I. Multiphase equation of state for carbon over wide range of temperatures and pressures. Int J Thermophys 2005;26(2):479–91. http://dx.doi.org/10.1007/s10765-005-4510-0.

[30] Correa AA, Benedict LX, Young DA, Schwegler E, Bonev SA. First-principles multiphase equation of state of carbon under extreme conditions. Phys Rev B 2008;78:024101. http://dx.doi.org/10.1103/PhysRevB.78.024101.

[31] Stuart SJ, Tutein AB, Harrison JA. A reactive potential for hydrocarbons with intermolecular interactions. J Chem Phys 2000;112(14):6472. http://dx.doi.org/10.1063/1.481208.

[32] Los JH, Fasolino A. Intrinsic long-range bond-order potential for carbon: performance in Monte Carlo simulations of graphitization. Phys Rev B 2003;68(2):1–14. http://dx.doi.org/10.1103/PhysRevB.68.024107.

[33] Wu CJ, Glosli JN, Galli G, Ree FH. Liquid–liquid phase transition in elemental carbon: a first-principles investigation. Phys Rev Lett 2002;89:135701. http://dx.doi.org/10.1103/PhysRevLett.89.135701.

[34] Kum O, Ree FH, Stuart SJ, Wu CJ. Molecular dynamics investigation on liquid–liquid phase change in carbon with empirical bond-order potentials. J Chem Phys 2003;119(12):6053–6. http://dx.doi.org/10.1063/1.1601216.

[35] Ghiringhelli LM, Valeriani C, Los JH, Meijer EJ, Fasolino A, Frenkel D. State-of-the-art models for the phase diagram of carbon and diamond nucleation. Mol Phys 2008;106(16–18):2011–38. http://dx.doi.org/10.1080/00268970802077884.

[36] Ghiringhelli LM, Los JH, Meijer EJ, Fasolino A, Frenkel D. Modeling the phase diagram of carbon. Phys Rev Lett 2005;94(14):145701. http://dx.doi.org/10.1103/PhysRevLett.94.145701.

[37] Colonna F, Los JH, Fasolino A, Meijer EJ. Properties of graphite at melting from multilayer thermodynamic integration. Phys Rev B 2009;80(13):1–8. http://dx.doi.org/10.1103/PhysRevB.80.134103.

[38] Lutsko JF, Wolf D, Phillpot SR, Yip S. Molecular-dynamics study of lattice-defect-nucleated melting in metals using an embedded-atom-method potential. Phys Rev B 1989;40(5):2841–55. http://dx.doi.org/10.1103/PhysRevB.40.2841.

[39] Stegailov VV. Homogeneous and heterogeneous mechanisms of superheated solid melting and decay. Comput Phys Commun 2005;169:247–50. http://dx.doi.org/10.1016/j.cpc.2005.03.057.

[40] Lu K, Li Y. Homogeneous nucleation catastrophe as a kinetic stability limit for superheated crystal. Phys Rev Lett 1998;80:4474–7. http://dx.doi.org/10.1103/PhysRevLett.80.4474.

[41] Luo S-N, Ahrens TJ, Çğian T, Strachan A, Goddard III WA, Swift DC. Maximum superheating and undercooling: systematics, molecular dynamics simulations, and dynamic experiments. Phys Rev B 2003;68:134206. http://dx.doi.org/10.1103/PhysRevB.68.134206.

[42] Kuksin AY, Norman GE, Stegailov VV, Yanilkin AV. Surface melting of superheated crystals. Atomistic simulation study. Comput Phys Commun 2007;177(12):34–7. http://dx.doi.org/10.1016/j.cpc.2007.02.073.

[43] Maltsev I, Mirzoev A, Danilov D, Nestler B. Atomistic and mesoscale simulations of free solidification in comparison. Model Simul Mater Sci Eng 2009;17(5):055006. http://dx.doi.org/10.1088/0965-0393/17/5/055006.

[44] Monk J, Yang Y, Mendelev MI, Asta M, Hoyt JJ, Sun DY. Determination of the crystal–melt interface kinetic coefficient from molecular dynamics simulations. Model Simul Mater Sci Eng 2010;18(1):015004. http://dx.doi.org/10.1088/0965-0393/18/1/015004.

[45] Plimpton SJ. Fast parallel algorithms for short-range molecular dynamics. J Comput Phys 1995;117(1):1–19. http://dx.doi.org/10.1006/jcph.1995.1039. URL: http://lammps.sandia.gov http://linkinghub.elsevier.com/retrieve/pii/S002199918571039X.

[46] Plimpton SJ, Thompson AP. Computational aspects of many-body potentials. MRS Bull 2012;37(1):513–21. http://dx.doi.org/10.1557/mrs.2012.96. URL: http://journals.cambridge.org/article_S0883769412000966.

[47] Martyna GJ, Tobias DJ, Klein ML. Constant pressure molecular dynamics algorithms. J Chem Phys 1994;101(5):4177–89. http://dx.doi.org/10.1063/1.467468.

[48] Orekhov ND, Stegailov VV. Molecular dynamics simulation of graphite melting. High Temp 2014;52(2):220–8. http://dx.doi.org/10.1134/S0018151X14020187.

[49] Grochola G. Constrained fluid λ-integration: constructing a reversible thermodynamic path between the solid and liquid state. J Chem Phys 2004;120(5):2122–6. http://dx.doi.org/10.1063/1.1637575.

[50] Broughton JQ, Gilmer GH, Jackson KA. Crystallization rates of a Lennard-Jones liquid. Phys Rev Lett 1982;49:1496–500. http://dx.doi.org/10.1103/PhysRevLett.49.1496.

[51] Mikheev LV, Chernov AA. Mobility of a diffuse simple crystal–melt interface. J Cryst Growth 1991;112(23):591–6. http://dx.doi.org/10.1016/0022-0248(91)90340-B.

[52] Sun DY, Asta M, Hoyt JJ. Kinetic coefficient of Ni solid–liquid interfaces from molecular-dynamics simulations. Phys Rev B 2004;69:024108. http://dx.doi.org/10.1103/PhysRevB.69.024108.

[53] Jackson K. Kinetic processes: crystal growth, diffusion, and phase transitions in materials. Weinheim: Wiley-VCH; 2004.

[54] De Sorbo W, Tyler WW. The specific heat of graphite from 13 to 300 K. J Chem Phys 1953;21(10):1660–3. http://dx.doi.org/10.1063/1.1698640.

[55] Li L, Reich S, Robertson J. Defect energies of graphite: density-functional calculations. Phys Rev B 2005;72(18):184109. http://dx.doi.org/10.1103/PhysRevB.72.184109.

[56] Norman GE, Stegailov VV. Homogeneous nucleation in a superheated crystal. Molecular-dynamic simulation. Dokl Phys 2002;47(9):667–71.

[57] Kuksin AY, Norman GE, Pisarev VV, Stegailov VV, Yanilkin AV. Theory and molecular dynamics modeling of spall fracture in liquids. Phys Rev B 2010;82:174101. http://dx.doi.org/10.1103/PhysRevB.82.174101.

[58] Baidakov VG, Bobrov KS. Spontaneous cavitation in a Lennard-Jones liquid at negative pressures. J Chem Phys 2014;140(18):184506. http://dx.doi.org/10.1063/1.4874644.

[59] Zakharchenko KV, Fasolino A, Los JH, Katsnelson MI. Melting of graphene: from two to one dimension. J Phys Condens Matter 2011;23(20):202202. http://dx.doi.org/10.1088/0953-8984/23/20/202202.